Journal of Molecular Catalysis A: Chemical 377 (2013) 162–172

Contents lists available at SciVerse ScienceDirect

Journal of Molecular Catalysis A: Chemical

journal homepage: www.elsevier.com/locate/molcata

Editor's choice paper

Relating cumene hydrocracking activity to the acidic center of CrO_3–ZrO_2

N.H.R. Annuar[a], A.A. Jalil[b], S. Triwahyono[a,c,*], Z. Ramli[a]

[a] Department of Chemistry, Faculty of Science, Universiti Teknologi Malaysia, 81310 UTM Johor Bahru, Johor, Malaysia
[b] Institute of Hydrogen Economy, Faculty of Chemical Engineering, Universiti Teknologi Malaysia, 81310 UTM Johor Bahru, Johor, Malaysia
[c] Ibnu Sina Institute for Fundamental Science Studies, Universiti Teknologi Malaysia, 81310 UTM Johor Bahru, Johor, Malaysia

ARTICLE INFO

Article history:
Received 28 February 2013
Received in revised form 6 May 2013
Accepted 7 May 2013
Available online xxx

Keywords:
CrO_3–ZrO_2
Brønsted acidic center
Lewis acidic center
Cumene cracking
n-Heptane isomerization

ABSTRACT

The properties of CrO_3–ZrO_2 and Pt/CrO_3–ZrO_2 were studied by IR and ESR spectroscopy to elucidate the active sites in *n*-heptane isomerization and cumene cracking. Surface analyses showed the presence of cubic, monoclinic and tetragonal phases of ZrO_2 with a BET specific surface area of about 150 m^2/g for both catalysts. 2,6-Lutidine adsorbed IR confirmed the presence of treble doublet bands at 1675 + 1660, 1650 + 1625 and 1640 + 1630 cm^{-1} corresponding to Brønsted acid sites and quartet doublet bands at 1604 + 1580, 1595 + 1580, 1590 + 1580 and 1570 + 1560 cm^{-1} corresponding to Lewis acid sites. The presence of Pt enhanced the activity of CrO_3–ZrO_2 in cumene hydrocracking, in which Pt facilitated the formation of protonic acid sites at 1675 + 1660 and 1650 + 1625 cm^{-1} through a hydrogen spillover mechanism. The IR study verified that the Lewis acidic center at 1570 + 1560 cm^{-1} was involved in the formation of protons by trapping electrons. Meanwhile, neither CrO_3–ZrO_2 nor Pt/CrO_3–ZrO_2 was active in *n*-heptane hydroisomerization.

1. Introduction

The acidic nature of ZrO_2 solid oxides has been found to have an excellent effect on acid catalytic reactions. The acidic properties of ZrO_2 can be improved by admixtures of oxoanions of p and d elements. They do not form bulk solutions with ZrO_2, but they modify the surface properties of ZrO_2 in terms of the thermal stability, crystallinity, surface area, pore distribution and acidity of ZrO_2 [1–4]. In recent years, various oxospecies like sulfate, chromate, carbonate, tungstate and molybdate supported on ZrO_2 have been widely explored in acid catalytic reactions such as alkane isomerization and cracking [5–7].

Chromium oxide-based catalysts have been studied for various petrochemical applications. These materials are also used for polymerization, hydrogenation and oxidation–reduction reactions between environmentally important molecules such as CO and NO. The structure and reactivity are altered when chromium oxide is supported on other metal oxides such as ZrO_2, Al_2O_3, SiO_2 and TiO_2 [8]. De Rossi et al. reported that Cr–ZrO_2 catalysts exhibit higher activity in isobutene dehydrogenation than those of similarly prepared Cr–Al_2O_3 and Cr–SiO_2 materials due to the stabilization of the high surface area of ZrO_2 at the working temperature [9]. Sohn et al. studied the combination of ZrO_2 and CrO_x, which probably generates stronger acid sites and more acidity as compared with the separate components [10]. They reported on pyridine adsorption on solid surfaces where it was possible to distinguish between Brønsted and Lewis acid sites. Bands at 1554 and 1497 cm^{-1} were found to be the characteristic peaks of pyridinium ions bonded to Brønsted acid sites, while the other set of absorption peaks at 1443, 1483, 1580 and 1605 cm^{-1} were contributed by pyridine coordinatively bonded to Lewis acid sites.

Although previous studies have investigated the CrO_3–ZrO_2 catalyst, there is currently a lack of published reports related to the acidity of CrO_3–ZrO_2 and Pt/CrO_3–ZrO_2. In the present study, we report the acidic center–catalytic activity relationship of CrO_3–ZrO_2 type catalysts in *n*-heptane hydroisomerization and cumene hydrocracking. 2,6-Lutidine was used as a basic probe molecule to evaluate the acidic properties of the catalysts. 2,6-Lutidine is used widely to evaluate the acidity of catalysts, particularly in the observation of the relatively weak Brønsted acid sites and the acidic centers of Lewis acid site types due to stronger basic property than pyridine [11–13]. Hydrogen adsorbed IR and ESR spectroscopy were used to observe the participation of acidic centers in the formation of protons and electrons from molecular hydrogen at elevated temperature. Similarities and differences in the acidity and activity of WO_3–ZrO_2, MoO_3–ZrO_2 and CrO_3–ZrO_2 catalysts are also discussed.

* Corresponding author at: Ibnu Sina Institute for Fundamental Science Studies, Universiti Teknologi Malaysia, 81310 UTM Johor Bahru, Johor, Malaysia.
Tel.: +60 7 5536076; fax: +60 7 5536080.
E-mail addresses: sugeng@utm.my, sugengtw@gmail.com (S. Triwahyono).

1381-1169/$ – see front matter © 2013 Elsevier B.V. All rights reserved.
http://dx.doi.org/10.1016/j.molcata.2013.05.008

2. Experimental

2.1. Catalysts preparation

Zirconium hydroxide ($Zr(OH)_4$) was prepared from an aqueous solution of $ZrOCl_2{\cdot}8H_2O$ (Wako Pure Chemical) by hydrolysis with 2.5 wt% NH_4OH (Merck) aqueous solution [7]. The final pH value of the supernatant was 9.0. The precipitate was filtered and washed with double deionized water. The gel obtained was dried at 383 K to form $Zr(OH)_4$. Chromium(VI) oxide supported on zirconia (CrO_3–ZrO_2) catalyst was prepared by incipient wetness impregnation technique of $Zr(OH)_4$ with chromium nitrate nonahydrate ($Cr(NO_3)_3{\cdot}9H_2O$, Merck), followed by drying overnight and calcination at 873 K for 3 h in air. The BET specific surface area of CrO_3–ZrO_2 was 150 m^2/g and the content of CrO_3 was 8 wt%. The Pt/CrO_3–ZrO_2 catalyst was prepared by impregnation of the CrO_3–ZrO_2 with aqueous solution of hydrogen hexachloroplatinate hydrate ($H_2PtCl_6{\cdot}6H_2O$, Aldrich) followed by drying overnight and calcination at 873 K for 3 h in air. The BET specific surface area of Pt/CrO_3–ZrO_2 was 147 m^2/g and content of Pt was 0.5 wt%.

2.2. Characterization of catalyst

X-ray diffraction (XRD) analysis was used to measure the crystallinity of the sample with a Bruker Advance D8 X-ray powder diffractometer with Cu Kα (λ = 1.5418 Å) radiation as the diffracted monochromatic beam at 40 kV and 40 mA. The data were collected over the range of $2\theta = 2$–40° with a scan rate of 0.025° continuously. The volume fraction of tetragonal or cubic and monoclinic phases of ZrO_2 was determined based on Toraya equation [14]:

$$V_{t,c} = 1 - \frac{1.31X_m}{1 + 0.31X_m} \quad (1)$$

$$X_m = \frac{I_m(1\,1\,\bar{1}) + I_m(1\,1\,1)}{I_m(1\,1\,\bar{1}) + I_m(1\,1\,1) + I_t(1\,1\,1)} \quad (2)$$

where X_m is the intensity ratio of monoclinic ZrO_2. $I_t(1\,1\,1)$, $I_m(1\,1\,1)$ and $I_m(1\,1\,\bar{1})$ are the integrated intensity of the (1 1 1) reflection of the tetragonal phase at $2\theta = 30.2^\circ$, (1 1 1) reflection of the monoclinic phase at $2\theta = 31.8^\circ$ and $(1\,1\,\bar{1})$ reflection of the monoclinic phase of ZrO_2 at $2\theta = 28.2^\circ$, respectively. For determination of the cubic phase of ZrO_2, the integrated intensity of (2 0 0) reflection of the cubic phase at $2\theta = 35.2^\circ$ was used to replace the $I_t(1\,1\,1)$ in Eq. (2). While 1.31 is the Toraya's theoretical deviation from linearity value [14].

The BET specific surface area of the catalysts was determined with a Quantachrome Autosorb-1 at 77 K. Prior to the analysis, the catalyst was outgassed at 573 K for 3 h.

For measurement of IR spectra, a self-supported wafer placed in an in situ IR cell was activated with a hydrogen stream at 598 K for 3 h, followed by outgassing at 598 K for 2 h [7,15]. 2,6-Lutidine was used as a basic probe molecule for evaluating of the acidity of sample. The activated sample was exposed to 0.53 kPa of 2,6-lutidine at room temperature, followed by outgassing at room temperature and 373 K. In the observation of the acidic strength, sample was activated at 473, 523 and 573 K before adsorption of 2,6-lutidine. In the hydrogen-exposure process, the 2,6-lutidine pre-adsorbed sample was exposed to 13.3 kPa of hydrogen at room temperature. The sample was then heated stepwise to 398 K in 25 K increments [16,17]. All spectra were recorded on an Agilent Carry 640 FTIR Spectrometer in a transmission mode at room temperature.

A JEOL JES-FA100 ESR spectrometer was used to observe the formation of unpaired electrons during the in vacuo heating and to observe the interaction of the unpaired electrons with electrons formed from molecular hydrogen at room temperature to 473 K. The catalyst was outgassed at 598 K for 3 h followed by the introduction of 6.7 kPa of gaseous hydrogen at room temperature [18]. Then the catalyst was heated to 323, 373, 423 and 473 K in the presence of hydrogen. All signals were recorded at room temperature.

2.3. Catalytic testing

Cumene cracking and *n*-heptane isomerization were carried out in a microcatalytic pulse reactor at temperature range of 373–573 K under hydrogen or helium stream. Prior to the reaction, 0.4 g portion of catalyst was charged into an ID10 mm tubular quartz glass reactor, and then was subjected to O_2 treatment at 673 K for 1 h, followed by H_2 reduction at 673 K for 3 h (H_2 = 100 mL/min). Then, the reactor was cooling down to a reaction temperature in the presence of H_2 stream. A dose of reactant was passed over the activated catalyst and the products were trapped at 77 K before being flash-evaporated into an online 6090 N Agilent Gas Chromatograph equipped with FID and TCD detectors. The intervals between doses were kept constant at 30 min.

The selectivity to particular product (S_i) and conversion of reactant ($X_{reactant}$) were calculated according to Eqs. (3) and (4), respectively.

$$S_i \ (\%) = \frac{C_i}{\sum C_i - C_{reactant}} \times 100 \quad (3)$$

$$X_{reactant} = \frac{\sum C_i - C_{reactant}}{\sum C_i} \quad (4)$$

where C_i and $C_{reactant}$ are mole number of particular compound and for residual reactant which was calculated based on the Scott hydrocarbon calibration standard gas (Air Liquide America Specialty Gases LLC). While, the specific rate conversion data was obtained by multiplication of the differential conversion data and rate constant (k). The rate constant was determined by the molar concentration of the reactant divided by mass of the catalyst per unit time with the assumption that the retention time for reactant in the catalyst bed was negligibly small.

3. Results and discussion

3.1. Physical properties of the catalysts

Fig. 1 shows the XRD patterns of ZrO_2, CrO_3–ZrO_2 and Pt/CrO_3–ZrO_2 catalysts that exhibited three well-established polymorphs which are the monoclinic, tetragonal and cubic phases of ZrO_2. The sharp diffraction lines observed at $2\theta = 24.2^\circ$, 28.1°, 31.4°, 33.9° and 38.4° correspond to the monoclinic phase of ZrO_2, while the peaks at $2\theta = 30.2^\circ$ and 35.5° correspond to the tetragonal phase of ZrO_2 [19,20]. The peak at $2\theta = 35.2^\circ$ corresponds to cubic phase of ZrO_2 [21]. The introduction of Cr(VI) partially eliminated and broadened the peaks assigned to the monoclinic and cubic phases of ZrO_2 and intensified the peaks corresponding to the tetragonal phase. In addition to the tetragonal phase of ZrO_2, new weak and broad peaks appeared at $2\theta = 24$–25°, assigned to bulk crystalline CrO_3, indicating the existence of free chromium(VI) oxide on the surface of ZrO_2 which formed bulk crystalline CrO_3 during calcination [22,23]. Similar to the findings of other studies, oxoanions such as SO_4^{2-}, WO_3 and MoO_3 and the presence of CrO_3 inhibited the sintering of ZrO_2 crystallites, which stabilized the tetragonal phase of ZrO_2 [17,24–26]. The fraction of tetragonal phase of ZrO_2 increased by about 34% with the introduction of CrO_3 whereas the fraction of cubic phase of ZrO_2 increased by about 10%. The addition of Pt on CrO_3–ZrO_2 did not have a considerable affect on the XRD pattern of CrO_3–ZrO_2 due to the stabilization of ZrO_2 already achieved by the incorporation of chromium(VI) oxide followed by

Table 1
Properties of ZrO_2, CrO_3–ZrO_2 and Pt/CrO_3–ZrO_2. The samples were activated at 573 K and outgassing of 2,6-lutidine at 373 K.

Sample	BET surface area (m^2/g)	M/T[a] phase of ZrO_2	M/C[b] phase of ZrO_2	Peak area of Brønsted acid sites[c]			Peak area of Lewis acid sites[c]			
				1675 + 1660	1650 + 1625	1640 + 1630	1604 + 1580	1595 + 1580	1590 + 1580	1570 + 1560
ZrO_2	42	83/17	90/10	0.0066	0.0043	0.0023	0.7059	0.0266	0.0453	0.0279
CrO_3–ZrO_2	150	49/51	80/20	0.4078	0.6600	0.4700	1.0000	3.0091	0.0073	0.8300
Pt/CrO_3–ZrO_2	147	48/52	80/20	0.4596	0.9200	0.9900	1.4900	2.6179	0.1076	0.7825

[a] Monoclinic/tetragonal.
[b] Monoclinic/cubic.
[c] Gaussian deconvolution area.

calcination. Table 1 shows the detailed properties of CrO_3–ZrO_2 type catalysts. The fraction of the tetragonal phase of ZrO_2 increased by about 35% with the introduction of CrO_3 and Pt. The fraction of the tetragonal phase was slightly higher for Pt/CrO_3–ZrO_2 than that for CrO_3–ZrO_2. Whereas the introduction of Pt on CrO_3–ZrO_2 did not change the fraction of cubic phase of ZrO_2. Iglesia and co-workers reported that tetragonal-to-monoclinic transformation of ZrO_2 occurs readily even at 298 K upon exposure to ambient air. Since the tetragonal-to-monoclinic transformation is a martensitic, diffusionless process, there is no activation barrier for the process [27]. The introduction of SO_4^{2-} converts most of the ZrO_2 into the tetragonal phase and the retained sulfate ions are mostly located on the ZrO_2 surface [28]. In the case of a W- or Mo-doped catalyst, the tungsten or molybdenum oxide exists as crystallites of WO_3 or MoO_3 and in the dispersed state along with the tetragonal form of ZrO_2. A study on a CrO_3–ZrO_2 catalyst was reported by Trunschke et al. in which the monoclinic and tetragonal phases of ZrO_2 existed together at low chromium loadings (0.5–2 wt%) [29,30]. The tetragonal phase of ZrO_2 predominated for 4 wt% chromium loading and above. Moreover, Sohn et al. revealed the influence of chromium oxide on the transition temperature of ZrO_2 from the tetragonal to the monoclinic phase [26]. The transition temperature increased in the range of 723–1173 K with an increasing chromium oxide content from 1 to 10 wt%; this could be explained in terms of a delay in the transition from the tetragonal to the monoclinic phase due to an increase in the number of chromium oxide molecules interacting with ZrO_2. While, the transition temperature of pure ZrO_2 into cubic phase is at above 2573 K.

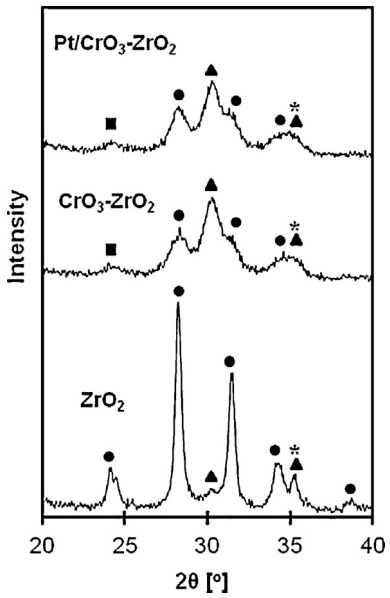

Fig. 1. X-ray diffraction patterns of ZrO_2, CrO_3–ZrO_2 and Pt/CrO_3–ZrO_2. (●) Monoclinic phase of ZrO_2; (▲) tetragonal phase of ZrO_2; (*) cubic phase of ZrO_2; and (■) bulk crystalline CrO_3.

The N_2 physisorption results show that the BET specific surface areas of ZrO_2, CrO_3–ZrO_2 and Pt/CrO_3–ZrO_2 were 42, 150 and 147 m^2/g, respectively (Table 1). This indicates that the introduction of CrO_3 and platinum increased the surface area of ZrO_2 due to an increase in the fraction of the tetragonal phase of ZrO_2 [31,32].

3.2. Intrinsic acidity of the catalysts

The 2,6-lutidine probe was used to study the acidity of CrO_3–ZrO_2 type catalysts due to the ability of 2,6-lutidine to distinguish between Brønsted and Lewis acid sites and to discriminate the variable strength of acidic centers [33,34]. Figs. 2 and 3 show the IR spectra of 2,6-lutidine adsorbed on activated ZrO_2, CrO_3–ZrO_2 and Pt/CrO_3–ZrO_2 and their Gaussian curve-fitting. The 2,6-lutidine was adsorbed on the catalysts at room temperature, followed by outgassing at 373 K. Curve-fitting was performed with six Gaussian peaks located at 1604, 1595, 1590, 1580, 1570 and 1560 cm^{-1} corresponding to the Lewis acidic center. For the Brønsted acidic center, six main Gaussian peaks were located at 1675, 1660, 1650, 1640, 1630 and 1625 cm^{-1}. It should be noted that the peak areas of the Lewis and Brønsted acidic centers for the parent ZrO_2 were lower than those of CrO_3–ZrO_2 and Pt/CrO_3–ZrO_2, indicating that the introduction of Cr(VI) and Pt modified the nature and concentration of the acidic centers. The parent ZrO_2 catalyst possessed a weak doublet band at 1650 + 1625 cm^{-1} ascribed to 2,6-lutidinium ions

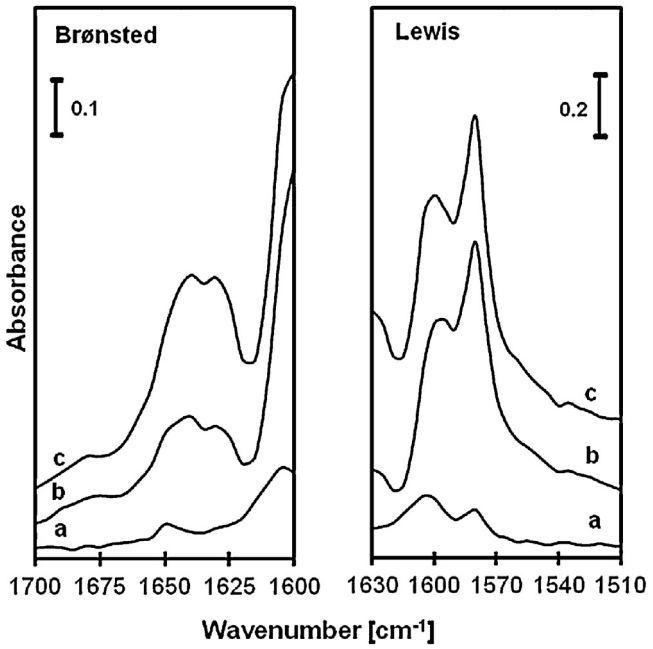

Fig. 2. IR spectra of 2,6-lutidine adsorbed on (a) ZrO_2, (b) CrO_3–ZrO_2 and (c) Pt/CrO_3–ZrO_2. Catalysts were activated at 573 K, followed by adsorption of 2,6-lutidine at RT and outgassing at 373 K.

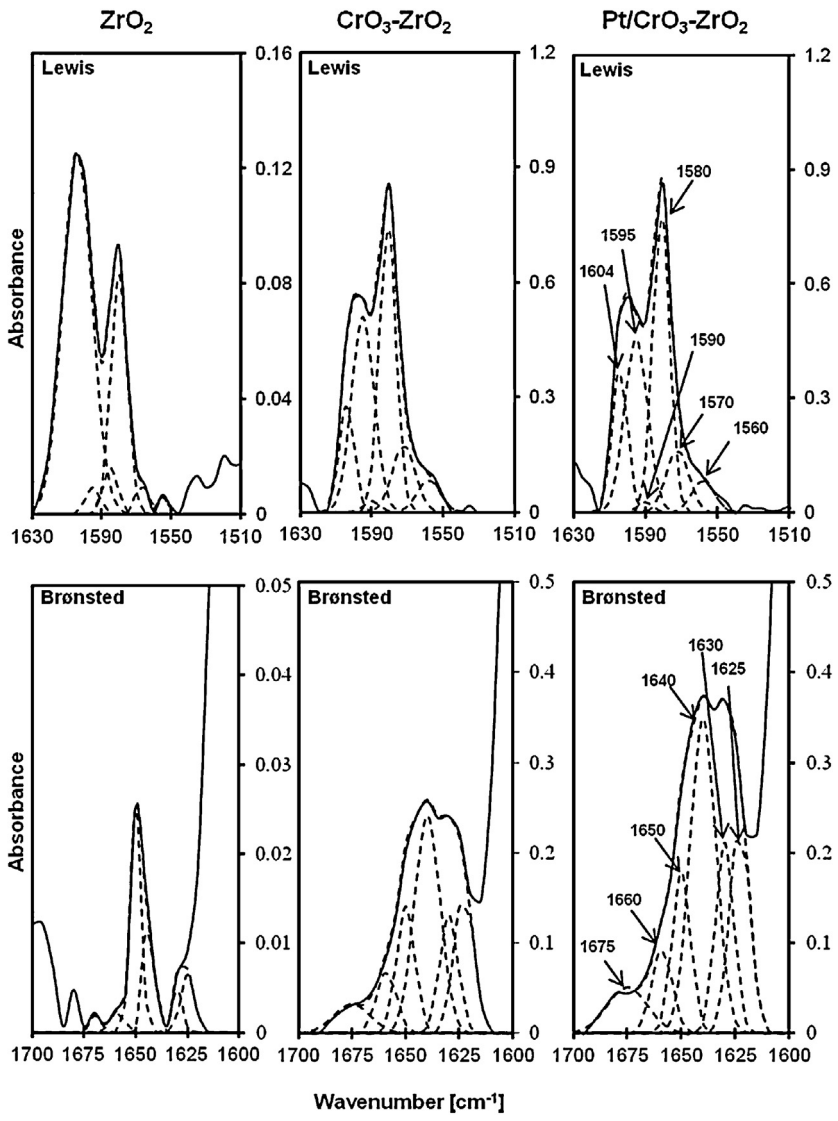

Fig. 3. Gaussian curve-fitting peaks of Lewis and Brønsted acid sites for ZrO_2, CrO_3–ZrO_2 and Pt/CrO_3–ZrO_2 in Fig. 2.

adsorbed on the Brønsted acidic center and a relatively weak doublet band at 1604 + 1580 cm^{-1} assigned to a physisorbed species or a species H-bonded to some surface OH groups. The latter doublet band is characteristic of the vibrations of 2,6-lutidine coordinated to a Lewis acidic center. The introduction of CrO_3 and Pt on ZrO_2 intensified the absorbance bands at 1650, 1625, 1604 and 1580 cm^{-1} and led to the development of new absorbance bands corresponding to the Lewis acidic center at 1595, 1590, 1570 and 1560 cm^{-1} and the Brønsted acidic center at 1675, 1660, 1640, 1630 and 1625 cm^{-1}.

Based on the literature data for 2,6-lutidine adsorption, the absorption bands on ZrO_2, CrO_3–ZrO_2 and Pt/CrO_3–ZrO_2 in this experiment can be summarized as follows [33–36]:

(i) For the ZrO_2 catalyst, the band ascribed to 8a and 8b ring vibrational modes of protonated 2,6-lutidine species was observed at 1650 and 1625 cm^{-1} for Brønsted acid sites. The doublet bands at 1604 cm^{-1} (8a mode) and 1580 cm^{-1} (8b mode) were assigned to physisorbed or H-bonded 2,6-lutidine on Lewis acid sites where the bands were attributed to the presence of the monoclinic phase of ZrO_2.

(ii) For the Brønsted acid region on the CrO_3–ZrO_2 and Pt/CrO_3–ZrO_2 catalysts, strong doublet bands appeared at 1640 cm^{-1} (8a mode) and 1630 cm^{-1} (8b mode) representing the protonated 2,6-lutidine species adsorbed on Brønsted acid sites. Shoulder bands at 1675 and 1660 cm^{-1} were due to the 8a and 8b ring vibrational modes, whereas the bands at 1650 cm^{-1} (8a mode) and 1625 cm^{-1} (8b mode) were assigned to the 2,6-lutidinium ions of Brønsted acid sites.

(iii) For the Lewis acid region on the CrO_3–ZrO_2 and Pt/CrO_3–ZrO_2 catalysts, dual doublets were observed, indicating H-bonded 2,6-lutidine corresponding to the monoclinic phase of ZrO_2. The first of these bands was seen at 1604 cm^{-1} (8a mode) and 1580 cm^{-1} (8b mode); the other was seen at 1590 cm^{-1} (8a mode) and 1580 cm^{-1} (8b mode). Furthermore, there were strong doublet bands corresponding to the tetragonal phase of ZrO_2 at 1595 cm^{-1} (8a mode) and 1580 cm^{-1} (8b mode). In addition, weak shoulder bands at 1570 cm^{-1} (8a mode) and 1560 cm^{-1} (8b mode) corresponding to the tetragonal phase of ZrO_2 were also observed.

The details of the doublet bands and the peak intensities for the ZrO_2, CrO_3–ZrO_2 and Pt/CrO_3–ZrO_2 catalysts are listed in Table 1. It is clearly shown that the presence of CrO_3 and Pt significantly increased the concentration of both Brønsted and Lewis acid sites, whereas the introduction of Pt on CrO_3–ZrO_2 increased

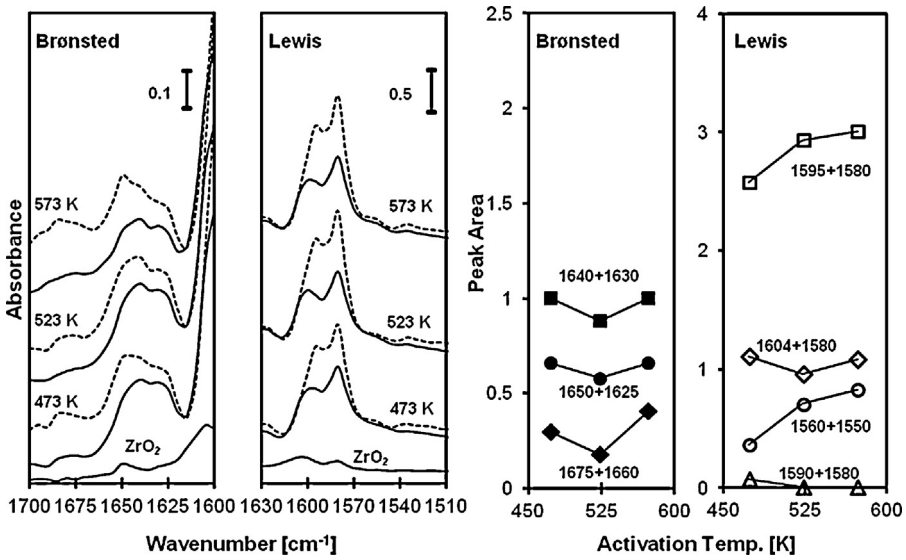

Fig. 4. IR spectra of 2,6-lutidine adsorbed CrO_3–ZrO_2 activated at different temperatures (473 K, 523 K and 573 K). 2,6-Lutidine was adsorbed at room temperature, followed by outgassing at room temperature (dotted lines) and 373 K (solid lines). The right figures show the changes in peak area of the Brønsted and Lewis acid sites according to the activation temperature of the sample.

the Brønsted acid sites but only slightly changed the Lewis acid sites.

Fig. 4 shows the IR spectra of 2,6-lutidine adsorbed on CrO_3–ZrO_2 activated at different temperatures of 473 K, 523 K and 573 K. 2,6-Lutidine was adsorbed on the activated sample at room temperature, followed by outgassing at room temperature and 373 K. The intensities of the bands decreased with an increase in the outgassing temperature of adsorbed 2,6-lutidine. These results indicate that CrO_3–ZrO_2 possesses strong Lewis and Brønsted acid sites which retain the 2,6-lutidine against outgassing at 373 K, while a considerable number of weak Lewis and Brønsted acid sites existed on which 2,6-lutidine was desorbed by outgassing at 373 K and below. It should be noted that the desorption of 2,6-lutidine bonded to Lewis acid sites occurred extensively for the sample activated at high temperature, indicating an increase in weak Lewis acid sites with increased activation temperature. However, the doublet bands at 1675 + 1660, 1650 + 1625 and 1640 + 1630 cm^{-1}, corresponding to Brønsted acid sites, were slightly decreased with increased activation temperature. These changes may have been caused by the removal of OH groups by a dehydration and/or dehydroxylation process which occurs easily at higher temperatures without modifying the Lewis acidic sites at 1595 + 1580 cm^{-1}, which correspond to the tetragonal phase of ZrO_2. In fact, there was no significant change in Lewis acid sites attributed to the monoclinic phase ZrO_2 at 1604 + 1580 and 1590 + 1580 cm^{-1} with a higher activation temperature.

The acidic properties were essentially the same for Pt/CrO_3–ZrO_2 as for CrO_3–ZrO_2. Fig. 5 shows the changes in the absorbance bands of the IR spectra as a function of the activation temperature and outgassing temperature of 2,6-lutidine for Pt/CrO_3–ZrO_2. Both Lewis and Brønsted acid sites decreased with increase in the outgassing temperature of 2,6-lutidine. For Lewis acid sites, the decrease was observed extensively for the samples activated at a low temperature, indicating the presence of abundant weak Lewis acid sites. The intensity of Brønsted acid sites decreased and, simultaneously, the intensity of Lewis acid sites increased as the activation temperature was raised. These gradual changes were observed at 1640 + 1630 and 1595 + 1580 cm^{-1}, attributed to acidic sites corresponding to the presence of the tetragonal phase of ZrO_2.

Several research groups have intensively studied the properties of acidic sites on ZrO_2 based catalysts. Onfroy et al. reported that the adsorption of 2,6-lutidine on ZrO_2 increased the bands at 1610 and 1580 cm^{-1} characteristic of Lewis acid sites while no Brønsted acid sites were detected [33]. The introduction of WO_x on ZrO_2 resulted in bands at 1644 and 1629 cm^{-1}, attributed to Brønsted acid sites. An increase in WO_x loading intensified the overall peaks in which all the peaks were retained against outgassing at 423 K; however, all peaks disappeared upon outgassing at 573 K [33]. In the case of the MoO_3–ZrO_2 catalyst, when the activation temperature increased, the absorbance bands assigned to Brønsted acid sites at 1640 and 1630 cm^{-1} decreased with a simultaneous increase in the absorbance bands assigned to Lewis acid sites at 1595 and 1580 cm^{-1} due to a dehydration and/or dehydroxylation process. This shows that when the catalysts were activated at high temperature, OH groups were eliminated, simultaneously leaving Lewis acid sites [16]. Study the acidity and acid strength of CrO_x/ZrO_2 was reported by Sohn et al. in which pyridine adsorption IR and Hammet indicator testing showed that the introduction of chromium oxide developed strong acidic sites on ZrO_2 [10]. The acidity of CrO_x/ZrO_2 increased gradually in the introduction of chromium oxide up to 1.0 wt%, further introduction has increased the acidity to lesser extent.

Fig. 6 shows variations in the IR spectra in the Cr=O stretching region of the CrO_3–ZrO_2 and Pt/CrO_3–ZrO_2 catalysts activated at different temperatures (dotted lines), followed by 2,6-lutidine treatment (solid lines). Although the IR spectrum for Pt/CrO_3–ZrO_2 was slightly higher than that of CrO_3–ZrO_2, the band positions and structures resemble each other. Activation of both CrO_3–ZrO_2 and Pt/CrO_3–ZrO_2 catalysts at 473 K resulted in two absorbance bands at 1030 and 1010 cm^{-1} attributed to two independent Cr=O species. The absorbance bands corresponding to the symmetric and antisymmetric stretching modes of the O=Cr=O bond were not observed due to the absence of two absorbance bands with a wavenumber difference of 30–35 cm^{-1} [37]. Those two bands shifted to slightly higher frequencies by increasing the activation temperature; they appeared at 1035 and 1013 cm^{-1} with activation at 573 K. However, 2,6-lutidine treatment shifted these bands to lower frequencies (1018 and 985 cm^{-1}) due to the inductive effect by 2,6-lutidine coordinated to cus Zr^{4+} sites in the vicinity

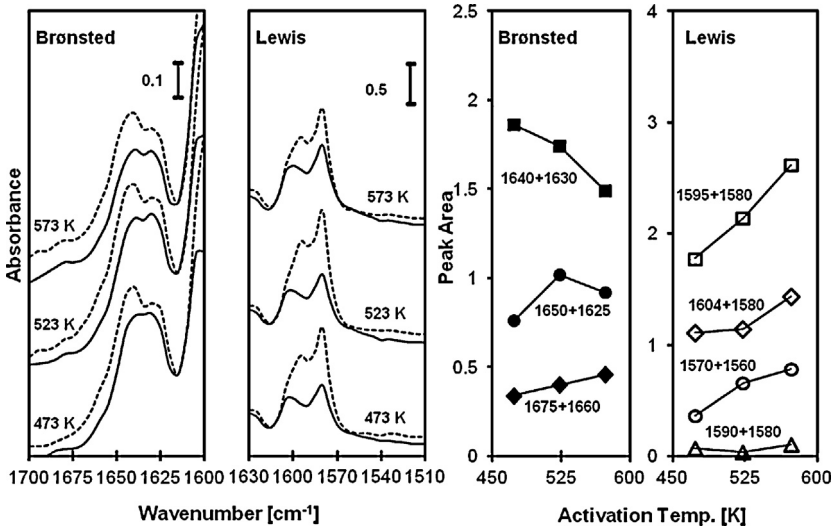

Fig. 5. IR spectra of 2,6-lutidine adsorbed $Pt/CrO_3–ZrO_2$ activated at different temperatures (473 K, 523 K and 573 K). 2,6-Lutidine was adsorbed at room temperature, followed by outgassing at room temperature (dotted lines) and 373 K (solid lines). The right figures show the changes in peak area of the Brønsted and Lewis acid sites according to the activation temperature of the sample.

of CrO_3. In addition, the absorbance band at 1013 cm^{-1} was more extensively affected than the other band at 1035 cm^{-1}. This result may indicate that the absorbance band at 1013 cm^{-1} should be assigned to Cr=O which is not directly connected to the cus Zr^{4+} Lewis acidic center but is rather connected to the other Cr through the O atom due to the properties of 2,6-lutidine, which is more sensitive toward Brønsted acidic sites. Thus, the band at 1035 cm^{-1} is assignable to the stretching of Cr=O which is connected to the cus Zr^{4+} Lewis acidic center through the O atom. The shift in the peaks of ZrO_2 based catalysts caused by the inductive effect of basic probe molecules such as pyridine and CO has also been reported for $WO_3–ZrO_2$ in which the interaction with the probe molecule shifted the peaks in the region of 1025–1014 cm^{-1} to 1015–980 cm^{-1} [31,37,38]. We concluded in our previous report on $WO_3–ZrO_2$ that the absorbance bands at higher frequencies should be attributed to the W=O stretching band which is connected to cus Zr^{4+}, whereas the stretching of W=O at a lower frequency can be attributed to a W=O stretching band which is connected to the other W through the O atom [37]. In addition, Scheithauer et al. also assessed the configuration of $WO_3–ZrO_2$ based on the results of IR and Raman spectra [31]. Two absorbance bands were observed in the W=O stretching region for the sample containing 8.6 wt% WO_3 at 1024 and 1015 cm^{-1} which were attributed to two independent W=O species.

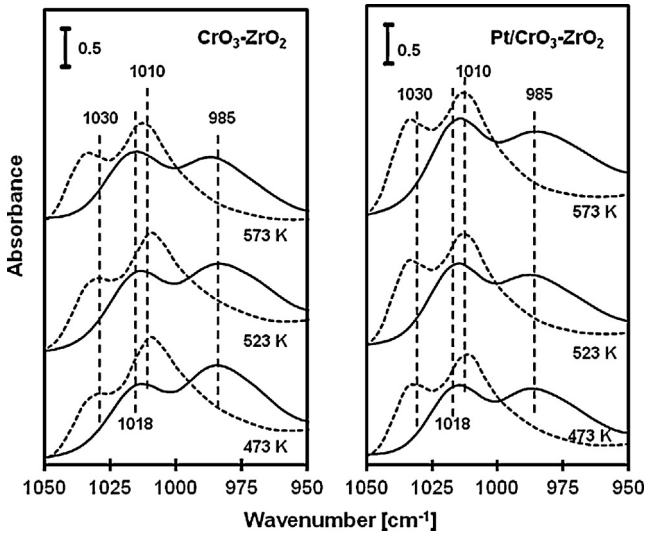

Fig. 6. IR spectra of 2,6-lutidine adsorbed $CrO_3–ZrO_2$ and $Pt/CrO_3–ZrO_2$ activated at different temperatures (473 K, 523 K and 573 K) (dotted lines). 2,6-Lutidine was adsorbed at room temperature, followed by outgassing at 373 K (solid lines).

3.3. Interaction of hydrogen and acidic surface of catalysts

Figs. 7 and 8 show the baseline correction of the IR spectra when 2,6-lutidine pre-adsorbed $CrO_3–ZrO_2$ and $Pt/CrO_3–ZrO_2$ catalysts were heated in the presence of 13.3 kPa hydrogen in a temperature range of 298–398 K. 2,6-Lutidine was adsorbed on the activated catalysts at room temperature followed by outgassing at 423 K. For $CrO_3–ZrO_2$ (Fig. 7), increasing the temperature in the presence of hydrogen gas did not significantly alter the absorbance bands. Based on the Gaussian curve-fitting, small changes were observed for the absorbance bands at 1675 + 1660 and 1650 + 1625 cm^{-1} attributed to the Brønsted acidic center, while a gradual increase was observed for the band at 1580 cm^{-1} attributed to physisorbed or H-bonded 2,6-lutidine on Lewis acid sites or the bulk species of ZrO_2 or CrO_3. In contrast, heating $Pt/CrO_3–ZrO_2$ in the presence of hydrogen gas markedly changed both Lewis and Brønsted acidic centers (Fig. 8).

Lewis acidic centers were markedly decreased and a simultaneous increase in Brønsted acidic centers was observed. In particular, a significant increase was observed in the bands at 1675 + 1660 and 1650 + 1625 cm^{-1} with a simultaneous decrease in the bands at 1570 + 1560 cm^{-1} [39]. Similar to the case of $CrO_3–ZrO_2$, the band at 1580 cm^{-1} increased with temperature for $Pt/CrO_3–ZrO_2$ as this band is related to physisorbed or H-bonded 2,6-lutidine on Lewis acid sites or bulk species of ZrO_2 or CrO_3.

These changes were more clearly seen when the absorbance bands were plotted against the heating temperature of the catalysts. These plots are shown in Fig. 9. For $CrO_3–ZrO_2$, double doublet bands corresponding to Brønsted acidic centers at 1675 + 1660 and 1650 + 1625 cm^{-1} increased to some extent at 373 K and above, which may have been due to the formation of protonic acid sites from molecular hydrogen. In contrast, there was almost no change in the absorbance bands corresponding to Lewis acidic centers. Although the band at 1580 cm^{-1} was considerably increased, this may have been related to the presence of physisorbed or

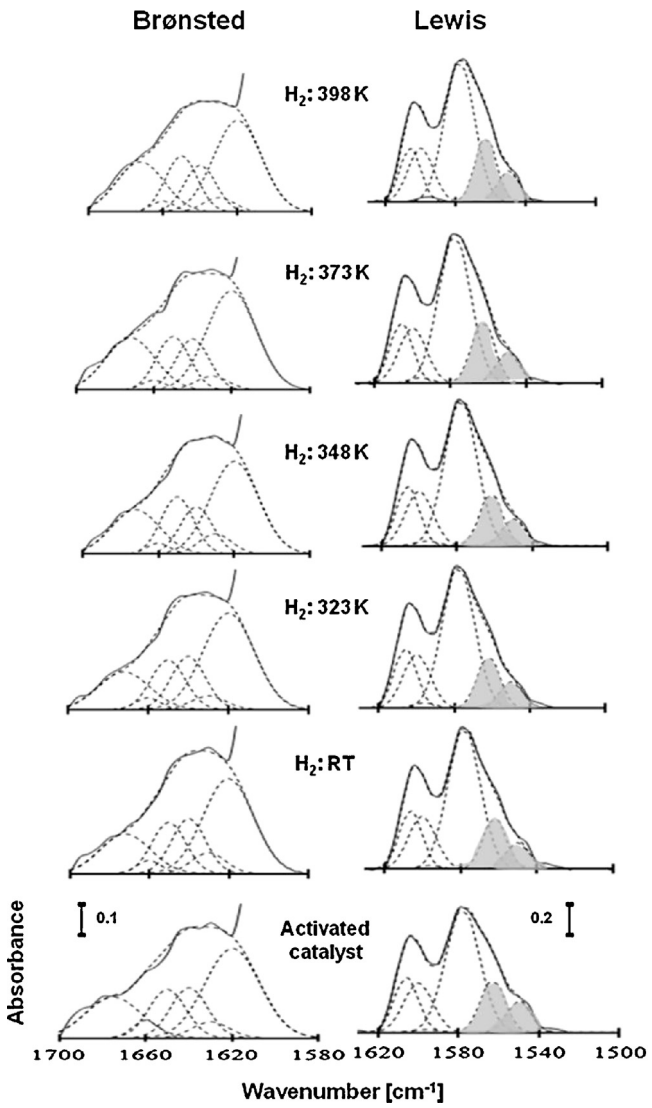

Fig. 7. Baseline correction of the IR spectra 2,6-lutidine adsorbed on activated CrO_3–ZrO_2 and Gaussian curve-fitting. Spectral changes occurred when 2,6-lutidine-pre-adsorbed CrO_3–ZrO_2 was heated in the presence of hydrogen at room temperature, 323 K, 348 K, 373 K and 398 K.

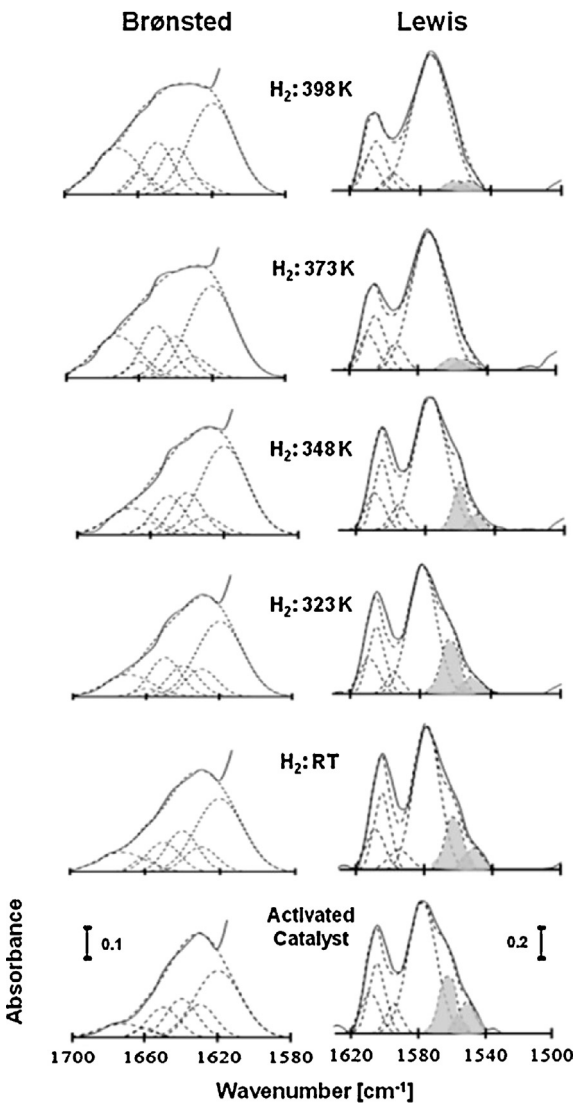

Fig. 8. Baseline correction of the IR spectra 2,6-lutidine adsorbed on activated Pt/CrO_3–ZrO_2 and Gaussian curve-fitting. Spectral changes occurred when 2,6-lutidine-pre-adsorbed Pt/CrO_3–ZrO_2 was heated in the presence of hydrogen at room temperature, 323 K, 348 K, 373 K and 398 K.

H-bonded 2,6-lutidine. The increase in this band at 1580 cm^{-1} was more extensively observed with Pt/CrO_3–ZrO_2 than with CrO_3–ZrO_2. The presence of Pt on CrO_3–ZrO_2 drastically improved the behavior of hydrogen interactions with the CrO_3–ZrO_2 catalyst. Heating Pt/CrO_3–ZrO_2 in the presence of hydrogen intensified the double doublet bands at 1675 + 1660 and 1650 + 1625 cm^{-1} attributed to Brønsted acidic centers at 298 K and above. Concurrently, the doublet absorbance band at 1570 + 1560 cm^{-1} attributed to Lewis acidic centers began to decrease at 298 K. The other absorbance bands at 1604, 1595, 1590 cm^{-1} started to decrease slightly at higher heating temperatures with a simultaneous imprecise increase in the doublet band at 1640 + 1630 cm^{-1}. These results obviously indicated that the presence of Pt is essential for CrO_3–ZrO_2 to facilitate the formation of protonic acid sites from molecular hydrogen. In fact, almost no protonic acid sites were formed with Pt-free CrO_3–ZrO_2 at relatively low temperatures. In addition to the Pt site, the presence of Lewis acidic centers at 1570 + 1560 cm^{-1} is required for the stabilization of protons by trapping electrons released from hydrogen atoms on the oxygen atom near the acidic center at 1570 + 1560 cm^{-1} [40].

Another difference between CrO_3–ZrO_2 and Pt/CrO_3–ZrO_2 was observed in the hydrogen adsorbed IR spectra in the Cr=O stretching region at 1050–950 cm^{-1} and the hydrogen adsorbed ESR spectra. Fig. 10 shows that heating CrO_3–ZrO_2 from room temperature to 398 K in the presence of hydrogen did not alter the bands at 1018 and 985 cm^{-1}, while the intensity of those peaks decreased and shifted toward lower frequencies for the Pt/CrO_3–ZrO_2, catalyst indicating that both Cr=O bands were affected by the presence of protonic acid sites formed from molecular hydrogen.

A different phenomenon was observed in the formation of electrons from molecular hydrogen over CrO_3–ZrO_2 and Pt/CrO_3–ZrO_2, as shown in the ESR spectra (Figs. 11 and 12). Heating both the CrO_3–ZrO_2 and Pt/CrO_3–ZrO_2 catalysts in a vacuum formed unpaired electrons at $g = 1.96$ and $g = 1.93$ associated with the desorption of hydroxyl groups from the surface of the catalyst, which subsequently left electron-deficient metal cations and/or oxygen radicals [18]. The signal appearing at $g = 1.96$ signifies that the O_2^- radical is connected to the tetrahedral Cr^{6+} species to form a Cr^{6+}–O_2^- complex [41]. The low signal at $g = 1.93$ may be due to electron-deficient metal cations which corresponds to unpaired electrons that have localized on metal cations [42]. Fig. 11

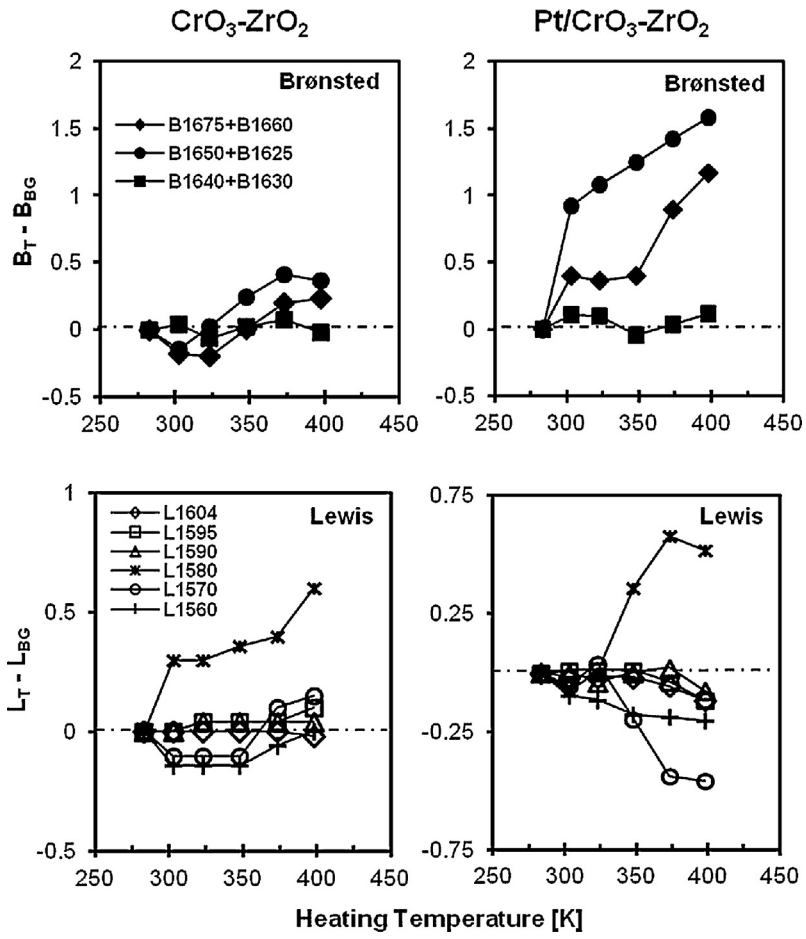

Fig. 9. Changes in absorbance for the Brønsted and Lewis acid sites upon heating in hydrogen for CrO_3–ZrO_2 and Pt/CrO_3–ZrO_2.

shows the ESR signal after heating the catalysts in the presence of hydrogen. When CrO_3–ZrO_2 and Pt/CrO_3–ZrO_2 catalysts were heated in the presence of hydrogen, the signal at $g = 1.96$ decreased slightly due to the formation of electrons which then interacted with the Cr^{6+}–O_2^- complex. For the signal at $g = 1.93$, there was almost no change for the CrO_3–ZrO_2 catalyst while a significant decrease was observed for Pt/CrO_3–ZrO_2 due to the interaction of electron-deficient metal cations and electrons upon heating in the presence of hydrogen. The variations of the intensity of ESR signals for both CrO_3–ZrO_2 and Pt/CrO_3–ZrO_2 catalysts are shown in Fig. 12. A similar trend was observed in the ESR signal at $g = 1.96$ for both the CrO_3–ZrO_2 and Pt/CrO_3–ZrO_2 catalysts upon heating in the

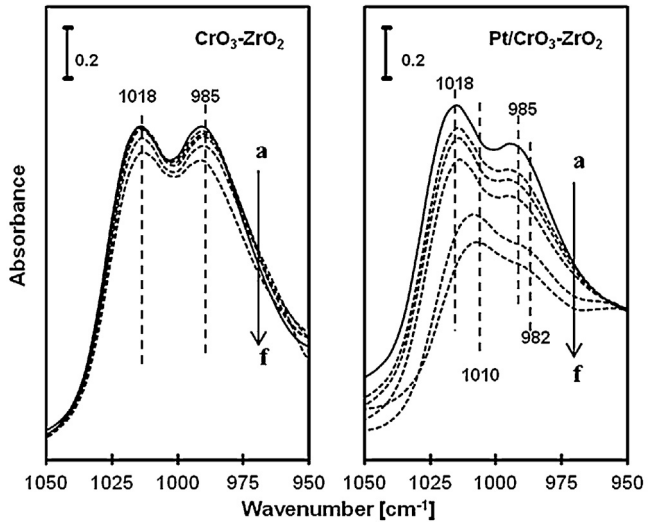

Fig. 10. IR spectra of 2,6-lutidine adsorbed on activated CrO_3–ZrO_2 and Pt/CrO_3–ZrO_2. Spectral changes occurred when 2,6-lutidine-pre-adsorbed CrO_3–ZrO_2 and Pt/CrO_3–ZrO_2 were heated in hydrogen at (b) room temperature, (c) 323 K, (d) 348 K, (e) 373 K and (f) 398 K (dotted lines). (a) Before adsorption with hydrogen (solid line).

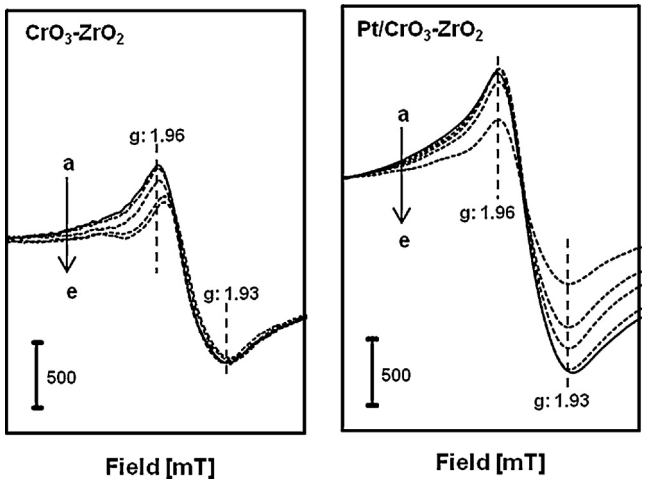

Fig. 11. ESR spectra of CrO_3–ZrO_2 and Pt/CrO_3–ZrO_2 activated at (a) 673 K for 1 h. 6.7 kPa of hydrogen was adsorbed at (b) 323 K, (c) 373 K, (d) 423 K and (e) 473 K.

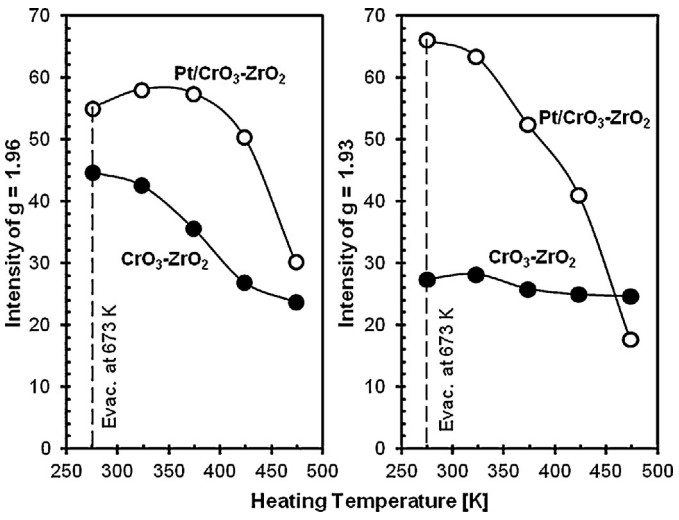

Fig. 12. Variations in the intensity of the ESR signal at $g = 1.96$ and $g = 1.93$ as a function of heating temperature. The dotted line represents the intensity of signals before the samples were heated in the presence of hydrogen.

presence of hydrogen. The signal decreased slightly with increasing of heating temperature, indicating an increase in the interaction of unpaired electrons with electrons formed from molecular hydrogen. A different phenomenon was observed in the ESR signal at $g = 1.93$ in which the signal did not change much for CrO_3–ZrO_2, although the signal decreased intensely for the Pt/CrO_3–ZrO_2 catalyst. These results reveal that the presence of Pt enhances the formation of electrons from atomic hydrogen which then interact with unpaired electrons at $g = 1.93$ [43]. Pt was used as a promoter for this kind of heterogeneous catalyst [44–46]. In general, these results confirm that the interaction of molecular hydrogen with Pt/CrO_3–ZrO_2 formed protonic acid sites and electrons through a hydrogen spillover mechanism. Molecular hydrogen is adsorbed on Pt sites to form hydrogen atoms that spillover onto the surface of CrO_3–ZrO_2 and undergo surface diffusion. The spiltover hydrogen reaches a Lewis acidic center and donates an electron to form H^+. H^+ is then stabilized on atomic O near the Lewis acidic center. The Lewis acid site traps an electron which then reacts with a second spiltover hydrogen to form an H^- bond with a Lewis acid site [42]. In fact, the electron did not form at $g = 1.93$ for Pt-free CrO_3–ZrO_2, indicating the indispensability of Pt on CrO_3–ZrO_2 type catalysts.

We have also reported the interaction of molecular hydrogen with modified ZrO_2 and HZSM5 catalysts at elevated temperatures. The formation of protonic acid sites from molecular hydrogen over MoO_3–ZrO_2 was discussed based on the hydrogen adsorbed IR and ESR results [16,42]. Heating MoO_3–ZrO_2 in the presence of hydrogen gas intensified the IR absorbance bands at 1640 + 1630 cm^{-1} corresponding to protonic acid sites and decreased the bands at 1595 + 1580 cm^{-1} corresponding to Lewis acid sites. The ESR signals confirmed the formation of electrons during heating of the catalyst in the presence of hydrogen gas. Similarly, the interaction between molecular hydrogen and the WO_3–ZrO_2 catalyst to form protonic acid sites was confirmed by pyridine pre-adsorbed IR [5,47]. The phenomena observed for MoO_3 and WO_3 loaded on ZrO_2 are essentially the same as those observed for CrO_3 loaded on ZrO_2 in this report, though there are some differences among the MoO_3–ZrO_2, WO_3–ZrO_2 and CrO_3–ZrO_2 catalysts. While the presence of specific active sites such as Pt is indispensable for the formation of protonic acid sites from molecular hydrogen for CrO_3–ZrO_2, Pt sites are not necessary for MoO_3–ZrO_2 and WO_3–ZrO_2 in which molecular hydrogen may be dissociated over the metallic Mo/W or acidic sites [5,16,48]. The role of metal species in the formation of protonic acid sites from molecular hydrogen was studied on the modified HZSM5 catalyst [17,46]. The presence of metal species such as Pt and Ir formed more protonic acid sites than that of the parent HZSM5 due to the stabilization effect of metal species on H^+ by neutralizing electrons on nearby Lewis acid sites.

3.4. Catalytic testing

Fig. 13(A) and (B) shows the variations in cumene hydrocracking and *n*-heptane hydroisomerization as a function of reaction temperatures for the different catalysts. For cumene hydrocracking, the products were composed of propylene, benzene and trace amounts of toluene and ethylbenzene. Fig. 13(C) shows the rate conversion and product distribution of cumene hydrocracking over ZrO_2, CrO_3–ZrO_2, Pt/ZrO_2 and Pt/CrO_3–ZrO_2 at 523 K. Pt/CrO_3–ZrO_2 gave the highest rate conversion followed by Pt/ZrO_2, CrO_3–ZrO_2 and ZrO_2. For hydroisomerization of *n*-heptane, the outlet was composed of isoheptane and residual *n*-heptane for CrO_3–ZrO_2, Pt/ZrO_2 and Pt/CrO_3–ZrO_2 at 523 and below. C_1–C_4 cracking products and higher hydrocarbons were formed at 573 K for Pt/ZrO_2 and Pt/CrO_3–ZrO_2 catalysts due to the enhancement of thermal cracking. The parent ZrO_2 performed with zero activity within the entire reaction temperature range due to low acidity for initiating the reaction. Overall, Pt/CrO_3–ZrO_2 showed the highest activity for both cumene cracking and isomerization of *n*-heptane due to the role of Pt in facilitating the formation of protonic acid sites through a hydrogen spillover phenomenon. It should be noted that the rate conversion of cumene hydrocracking was almost 40 times greater than that of *n*-heptane hydroisomerization. The rate conversion of cumene was 30.1 μmol/s g-cat at 523 K, whereas the conversion was less than 0.77 μmol/s g-cat for *n*-heptane hydroisomerization. Although it is not certain at present what causes this difference in the activity of this catalyst in hydrocracking and hydroisomerization, it is plausible that the participation of acidic centers in the reaction determines the activity of the catalyst [49]. For the selectivity of cumene hydrocracking at 523 K, propylene showed a main contribution after loaded with Pt on CrO_3–ZrO_2 catalyst with 42.28% whereas benzene gives only 1.76% and 55.96% for trace amounts of toluene and ethylbenzene [50]. We have reported the role of acidic centers in the hydroisomerization of *n*-heptane over MoO_3 loaded on ZrO_2 in which Lewis acidic centers corresponding to the presence of the tetragonal phase of ZrO_2 at 1595 + 1580 cm^{-1} were responsible for the high activity in *n*-heptane isomerization [16]. Based on the 2,6-lutidine pre-adsorbed IR study on CrO_3–ZrO_2 catalysts, molecular hydrogen did not interact with Lewis acidic centers at 1604 + 1580, 1595 + 1580 or 1590 + 1580 cm^{-1}, but molecular hydrogen interacted with the doublet shoulder band at 1570 + 1560 cm^{-1} attributed to Lewis acidic centers corresponding to the presence of the tetragonal phase of ZrO_2. The acidic center at 1570 + 1560 cm^{-1} stabilized a proton on atomic oxygen by accepting an electron released from atomic hydrogen during the formation of a proton. The proton which formed through the interaction of molecular hydrogen with the acidic center at 1570 + 1560 cm^{-1} on CrO_3–ZrO_2 type catalysts was relatively inactive compared to that formed through the interaction with the acidic center at 1595 + 1580 cm^{-1} on MoO_3–ZrO_2. In fact, the MoO_3–ZrO_2 type catalyst was more active and stable than the CrO_3–ZrO_2 type in terms of *n*-heptane hydroisomerization. Although the Pt/CrO_3–ZrO_2 catalyst showed high activity and stability in cumene hydrocracking, CrO_3–ZrO_2 with or without Pt showed low activity in *n*-heptane hydroisomerization. The MO_3–ZrO_2 has also been examined in the cumene catalytic cracking in which increasing activation temperature and number of molybdenum oxide content improved the activity of catalyst due to the gradual increase in the surface acidity of catalyst [51].

Fig. 14(A) shows the changes in the activity of CrO_3–ZrO_2 and Pt/CrO_3–ZrO_2 in cumene cracking at 523 K as the carrier gas was

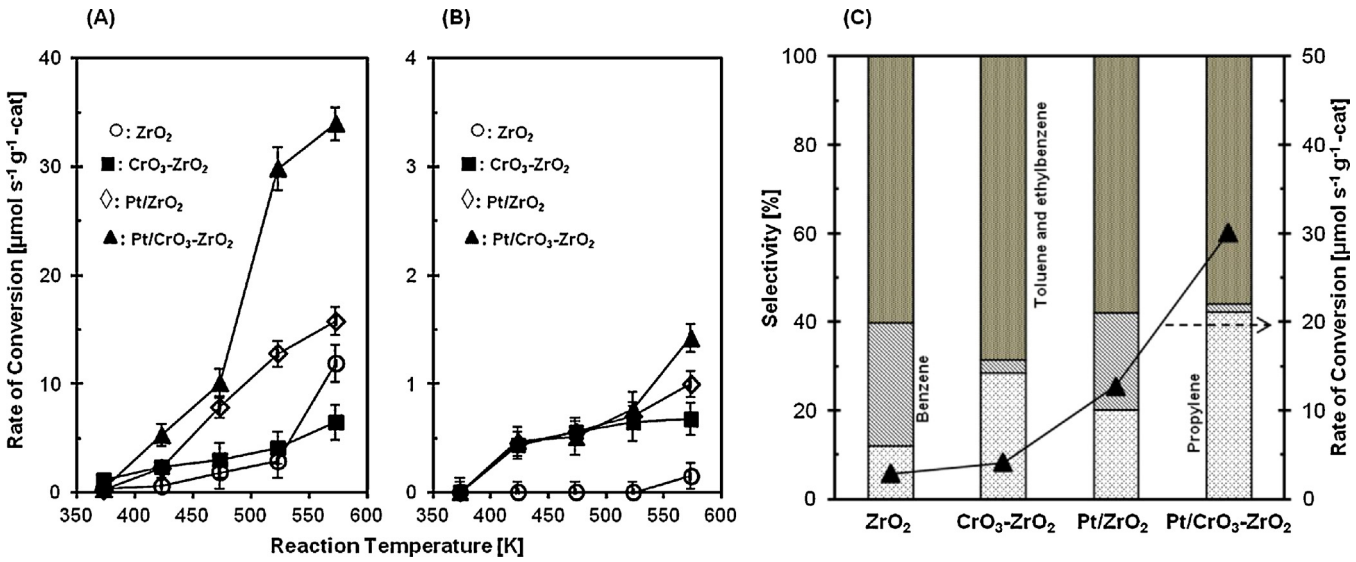

Fig. 13. Catalytic activity of ZrO_2, CrO_3–ZrO_2, Pt/ZrO_2 and Pt/CrO_3–ZrO_2 in (A) cumene hydrocracking and (B) *n*-heptane hydroisomerization in the presence of hydrogen. (C) Products distribution of cumene hydrocracking over ZrO_2, CrO_3–ZrO_2, Pt/ZrO_2 and Pt/CrO_3–ZrO_2 at 523 K.

sequentially switched from hydrogen to helium and vice versa. For CrO_3–ZrO_2, the rate conversion was about 3.5 μmol/s g-cat in the presence of hydrogen, which decreased to 2.1 μmol/s g-cat when the carrier gas was switched to helium. The activity slowly recovered to the original activity as the carrier gas was switched back to hydrogen. For Pt/CrO_3–ZrO_2, the presence of hydrogen gas in the first cycle enhanced and stabilized the catalytic activity of the catalyst where rate conversion reached more than 30.1 μmol/s g-cat. In the second cycle, the rate conversion decreased to about 2.2 μmol/s g-cat when the carrier gas was switched from hydrogen to helium. This decrease in the activity may have been due to the gradual exhaustion of protonic acid sites on the surface of Pt/CrO_3–ZrO_2 [44]. As the carrier gas was switched back to hydrogen, the activity and stability of Pt/CrO_3–ZrO_2 gradually recovered to the original activity. This confirmed that the high activity of Pt/CrO_3–ZrO_2 was due to the presence of protonic acid sites from molecular hydrogen which acted as catalytically active sites in the reaction. The promotion effects of molecular hydrogen in cumene cracking were also observed in a physical mixture of Pt/SiO_2 and HZSM5 as well as Pt/WO_3–ZrO_2 where the catalytic activities of these catalysts were higher in the presence of hydrogen [40,52]. In the presence of hydrogen carrier gas, the cumene conversion over the physical mixture of Pt/SiO_2 and HZSM5 was kept close to 100% in the initial reaction. As the hydrogen gas was switched into helium gas, the conversion rapidly decreased to some extent. This result clearly demonstrated the promotion effect of hydrogen in the cracking activity over the physical mixture of Pt/SiO_2 and HZSM5. Similar phenomenon was also observed on the Pt/WO_3–ZrO_2 in which changing of the hydrogen carrier gas to helium gas decreased the cracking activity of Pt/WO_3–ZrO_2.

Fig. 14(B) shows the IR spectra of fresh and used CrO_3–ZrO_2 and Pt/CrO_3–ZrO_2 catalysts under hydrogen and helium carrier gases. The IR spectra of fresh and used catalysts did not change significantly for both catalysts. This manifested that CrO_3–ZrO_2 and Pt/CrO_3–ZrO_2 do not form any coke and carbonaceous species during the reaction under the presence of hydrogen or helium

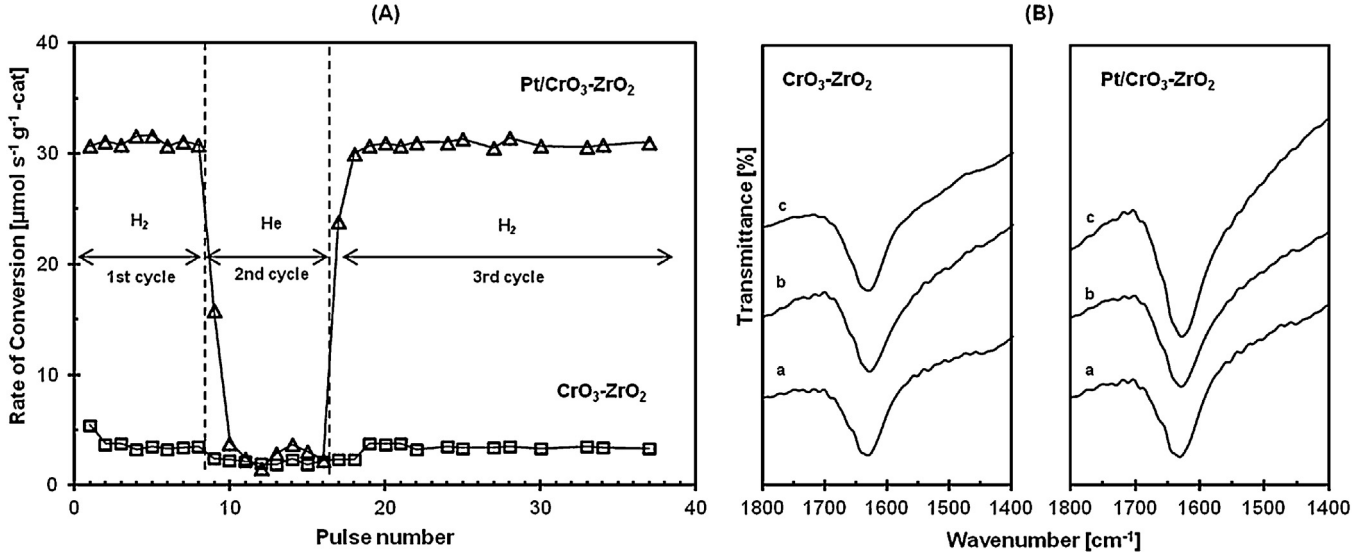

Fig. 14. (A) Activity and stability of CrO_3–ZrO_2 and Pt/CrO_3–ZrO_2 in cumene cracking in the presence of hydrogen or helium gas at 523 K. (B) IR spectra of CrO_3–ZrO_2 and Pt/CrO_3–ZrO_2; (a) fresh catalyst, (b) after cumene cracking in the presence of hydrogen and (c) after cumene cracking in the presence of helium.

carrier gas. This result strongly suggested that the low activity of $Pt/CrO_3–ZrO_2$ in the presence of helium carrier gas was not caused by the formation of coke deposits on the surface catalyst but it was due to the absence of protonic acid sites during the reaction.

4. Conclusion

The 2,6-lutidine pre-adsorbed IR spectra revealed the presence of doublet bands at 1675 + 1660, 1650 + 1625 and 1640 + 1630 cm^{-1} for Brønsted acid sites and doublet bands at 1604 + 1580, 1595 + 1580, 1590 + 1580 and 1570 + 1560 cm^{-1} for Lewis acid sites on the $CrO_3–ZrO_2$ and $Pt/CrO_3–ZrO_2$ catalysts. Both the Brønsted and Lewis acid sites were strong; 2,6-lutidine remained after heating in a vacuum at 423 K. In addition, there existed a number of weak acidic sites from which the 2,6-lutidine was desorbed at 423 K and below.

The presence of Pt on $CrO_3–ZrO_2$ enhanced the activity in terms of cumene hydrocracking, but did not improve the activity in terms of *n*-heptane hydroisomerization. $CrO_3–ZrO_2$, Pt/ZrO_2 and ZrO_2 performed with low activity in both cumene hydrocracking and *n*-heptane hydroisomerization. Pt facilitated the formation of protonic acid sites through a hydrogen spillover mechanism in which the Lewis acidic centers at 1570 + 1560 cm^{-1} were involved in the stabilization of protonic acid sites. The other Lewis acidic centers at 1604 + 1580, 1595 + 1580 and 1590 + 1580 cm^{-1} did not interact with molecular hydrogen to form protonic acid sites. In addition, the presence of Brønsted acidic centers at 1640 + 1630 cm^{-1} did not considerably influence the activity of the catalyst. The formation of protonic acid sites from molecular hydrogen was also confirmed by the formation of electrons, as shown by the hydrogen adsorbed ESR study at elevated temperatures. These results suggest that the presence of specific active sites like Pt and Lewis acidic centers at 1570 + 1560 cm^{-1} and molecular hydrogen are indispensable in the acid catalytic reaction with $CrO_3–ZrO_2$ type catalysts.

Acknowledgements

This work was supported by the Universiti Teknologi Malaysia under Research University Grant no. 04H26. Our gratitude also goes to the Hitachi Scholarship Foundation for the Gas Chromatograph Instruments Grant.

References

[1] L. Osiglio, Á.G. Sathicq, G.P. Romanelli, M.N. Blanco, J. Mol. Catal. A: Chem. 359 (2012) 97–103.
[2] R. Cheng, C. Xu, Z. Liu, Q. Dong, X. He, Y. Fang, M. Terano, Y. Huc, T.J. Pullukat, B. Liu, J. Catal. 273 (2010) 103–115.
[3] P. Doggali, S. Waghmare, S. Rayalu, Y. Teraoka, N. Labhsetwar, J. Mol. Catal. A: Chem. 347 (2011) 52–59.
[4] G.D. Yadav, N.P. Ajgaonkar, A. Varma, J. Catal. 292 (2012) 99–110.
[5] S. Triwahyono, T. Yamada, H. Hattori, Appl. Catal. A 242 (2003) 101–109.
[6] S. Triwahyono, A.J. Aishah, S.N. Timmiati, N.N. Ruslan, H. Hattori, Appl. Catal. A 372 (2010) 103–107.
[7] S. Triwahyono, Z. Abdullah, A.J. Aishah, J. Nat. Gas. Chem. 15 (2006) 247–252.
[8] D.W. Flick, M.C. Huff, Appl. Catal. A 187 (1999) 13–24.
[9] S. De Rossi, M.P. Casaletto, G. Ferraris, A. Cimino, G. Minelli, Appl. Catal. A 167 (1998) 257–270.
[10] J.R. Sohn, S.G. Ryu, H.W. Kim, J. Mol. Catal. 135 (1998) 99–106.
[11] A. Corma, C. Rodelas, V. Fornes, J. Catal. 88 (1984) 374–381.
[12] C. Morterra, G. Cerrato, G. Meligrana, Langmuir 17 (2001) 7053–7060.
[13] F. Leydier, C. Chizallet, A. Chaumonnot, M. Digne, E. Soyer, A. Quoineaud, D. Costa, P. Raybaud, J. Catal. 284 (2011) 215–229.
[14] H. Toraya, M. Yoshimura, S. Sommiya, J. Am. Ceram. Soc. 67 (1984) 119–121.
[15] S. Triwahyono, T. Yamada, H. Hattori, Catal. Lett. 85 (2003) 109–115.
[16] N.N. Ruslan, N.A. Fadzlillah, A.H. Karim, A.J. Aishah, S. Triwahyono, Appl. Catal. A 406 (2011) 102–112.
[17] H.D. Setiabudi, A.J. Aishah, S. Triwahyono, N.H.N. Kamarudin, R.R. Mukti, Appl. Catal. A 417–418 (2012) 190–199.
[18] M.A.A. Aziz, N.H.N. Kamarudin, H.D. Setiabudi, H. Hamdan, A.A. Jalil, S. Triwahyono, J. Nat. Gas Chem. 21 (2012) 29–36.
[19] K. Achelhi, S. Masse, G. Laurent, R. Roux, A. Laghzizil, A. Saoiabi, T. Coradin, Langmuir 27 (2011) 15176–15184.
[20] L.F. Liotta, A.M. Venezia, G. Pantaleo, G. Deganello, M. Gruttadauria, R. Noto, Catal. Today 91–92 (2004) 231–236.
[21] B.L. Kirsch, A.E. Riley, A.F. Gross, S.H. Tolbert, Langmuir 20 (2004) 11247–11254.
[22] G. Stefanic, S. Music, A. Gajovic, J. Mol. Struct. 744–747 (2005) 541–549.
[23] J.R. Sohn, S.G. Ryu, Langmuir 9 (1993) 126–131.
[24] P. Wang, S. Yang, J.N. Kondo, K. Domen, T. Yamada, H. Hattori, J. Phys. Chem. B 107 (2003) 11951–11959.
[25] N. Soultanidis, W. Zhou, A.C. Psarras, A.J. Gonzalez, E.F. Iliopoulou, C.J. Kiely, I.E. Wachs, M.S. Wong, J. Am. Chem. Soc. 132 (2010) 13462–13471.
[26] J.R. Sohn, S.G. Ryu, M.Y. Park, Y.Il. Pae, J. Mater. Sci. 28 (1993) 4651–4659.
[27] S. Xie, E. Iglesia, A.T. Bell, Chem. Mater. 12 (2000) 2442–2447.
[28] B.M. Reddy, V.R. Reddy, J. Mater. Sci. Lett. 19 (2000) 763–765.
[29] A. Trunschke, D.L. Hoang, J. Radnik, H. Lieske, J. Catal. 191 (2000) 456–466.
[30] M.A. Vuurman, F.D. Hardcastle, I.E. Wachs, J. Mol. Catal. 84 (1993) 193–205.
[31] M. Scheithauer, R.K. Grasseli, H. Knozinger, Langmuir 14 (1998) 3019–3029.
[32] E.I. Ross-Medgaarden, W.V. Knowles, T. Kim, M.S. Wong, W. Zhou, C.J. Kiely, I.E. Wachs, J. Catal. 256 (2008) 108–125.
[33] T. Onfroy, G. Clet, M. Houalla, J. Phys. Chem. B 109 (2005) 3345–3354.
[34] V. Lebarbier, G. Clet, M. Houalla, J. Phys. Chem. B 110 (2006) 13905–13911.
[35] C. Morterra, G. Meligrana, G. Cerrato, V. Solinas, E. Rombi, M.F. Sini, Langmuir 19 (2003) 5344–5356.
[36] J.G. Santiesteban, J.C. Vartuli, S. Han, R.D. Bastian, C.D. Chang, J. Catal. 168 (1997) 431–441.
[37] S. Triwahyono, T. Yamada, H. Hattori, Appl. Catal. A 250 (2003) 75–81.
[38] T. Onfroy, V. Lebarbier, G. Clet, M. Houalla, J. Mol. Catal. A: Chem. 318 (2010) 1–7.
[39] V.B. Kazansky, A.I. Serykha, B.G. Andersonb, R.A. van Santen, Catal. Lett. 88 (2003) 3–4.
[40] H. Hattori, Stud. Surf. Sci. Catal. 138 (2001) 3–12.
[41] M. Selvaraj, S. Kawi, Microporous Mesoporous Mater. 101 (2007) 240–249.
[42] N.N. Ruslan, S. Triwahyono, A.J. Aishah, S.N. Timmiati, N.H.R. Annuar, Appl. Catal. A 413–414 (2012) 176–182.
[43] A. Punnoose, M.S. Seehra, Catal. Lett. 78 (2002) 1–4.
[44] Ü.B. Demirci, F. Garin, J. Mol. Catal. A: Chem. 188 (2002) 233–243.
[45] B. Wang, X. Wu, R. Ran, Z. Si, D. Weng, J. Mol. Catal. A: Chem. 361–362 (2012) 98–103.
[46] H.D. Setiabudi, A.A. Jalil, S. Triwahyono, J. Catal. 294 (2012) 128–135.
[47] A.H. Karim, S. Triwahyono, A.A. Jalil, H. Hattori, Appl. Catal. A 433–434 (2012) 49–57.
[48] H.D. Setiabudi, A.A. Jalil, S. Triwahyono, N.H.N. Kamarudin, R. Jusoh, Chem. Eng. J. 217 (2013) 300–309.
[49] T. Kitano, S. Okazaki, T. Shishido, K. Teramura, T. Tanaka, J. Mol. Catal. A: Chem. 371 (2013) 21–28.
[50] F. Seyedeyn Azad, J. Abedi, E. Salehi, T. Harding, Chem. Eng. J. 180 (2012) 145–150.
[51] E.A. El-Sharkawy, A.S. Khder, A.I. Ahmed, Microporous Mesoporous Mater. 102 (2007) 128–137.
[52] T.X. Cheng, H. Kabashima, H. Hattori, React. Kinet. Catal. Lett. 2 (2000) 201–207.